LAWRENCE
LIVERMORE
NATIONAL
LABORATORY

LLNL-CONF-679001

Energetic laser cleaning of metallic particles and surface damage on silica optics: Investigation of the underlying mechanisms

N. Shen, S. G. Demos, R. A. Negres, A. M. Rubenchik, C. D. Harris, M. J. Matthews

November 5, 2015

XLVII Annual Symposium on Optical Materials for High-Power Lasers
Boulder, CO, United States
September 27, 2015 through September 30, 2015

Disclaimer

Energetic laser cleaning of metallic particles and surface damage on silica optics: Investigation of the underlying mechanisms

Nan Shen, Stavros G. Demos, Raluca A. Negres, Alexander M, Rubenchik, Candace D. Harris[§] and Manyalibo J. Matthews

Lawrence Livermore National Laboratory, 7000 East Avenue, Livermore, CA 94550 USA

[§]Currently at the Department of Physics, Florida Agriculture and Mechanical University, Tallahassee, FL 32303 USA

[*]corresponding author nshen@llnl.gov

ABSTRACT

Surface particulate contamination on optics can lead to laser-induced damage hence limit the performance of high power laser system. In this work we focus on understanding the fundamental mechanisms that lead to damage initiation by metal contaminants. Using time resolved microscopy and plasma spectroscopy, we studied the dynamic process of ejecting ~30 μm stainless steel particles from the exit surface of fused silica substrate irradiated with 1064 nm, 10 ns and 355 nm, 8 ns laser pulses. Time-resolved plasma emission spectroscopy was used to characterize the energy coupling and temperature rise associated with single, 10-ns pulsed laser ablation of metallic particles bound to transparent substrates. Plasma associated with Fe(I) emission lines originating from steel microspheres was observe to cool from >24,000 K to ~15,000 K over ~220 ns as $\tau^{-0.22}$, consistent with radiative losses and adiabatic gas expansion of a relatively free plasma. Simultaneous emission lines from Si(II) associated with the plasma etching of the SiO_2 substrate were observed yielding higher plasma temperatures, ~35,000 K, relative to the Fe(I) plasma. The difference in species temperatures is consistent with plasma confinement at the microsphere-substrate interface as the particle is ejected, and is directly visualized using pump-probe shadowgraphy as a function of pulsed laser energy.

1. INTRODUCTION

Research in the area of surface cleaning of particulate contamination of microelectronics, [1] nuclear and plasma reactors[2,3] is driven by the need to quantify performance limitations. For example, particulate contamination on high power laser optics generated through optical processing and handling can lead to damage initiation and local fracture that, if left uncorrected, can limit optic lifetime in a pulsed laser system after a few successive shots.[4-6] Recent research[7] has revealed plasma pressure effects can lead to exacerbated surface pitting from metallic particles located on optic input surfaces. Particle-mediated laser-surface interactions have also been exploited to produce 'nano-jets' for processing of thin semiconductor membranes.[8] At high enough plasma temperatures and pressures a cross-over in behavior is observed whereby the surface modification and mechanical failure at the particle-substrate interface can be observed.[9,10] Therefore, characterization of the plasma produced during laser ablation of metal particles on optics could serve as an important tool in understanding *contaminant-mediated, laser-induced* surface pitting. Furthermore, capturing the time-resolved dynamics of the plasma formation and temperature rise could give further details of the relevant physical processes (e.g. plasma etching, evaporation or compaction).

Laser plasmas generated in the application of laser-induced breakdown spectroscopy (LIBS) are widely studied for the purpose of elemental analysis. Plasma characteristics depend on laser intensity, wavelength, and pulse duration, as well as on the physical and chemical characteristics of target material, and the surrounding atmosphere.[11] Electron and ionic temperatures are of particular interest in defining the plasma characteristics since energy balance can be used to understand the laser-matter interactions driving ablation. Because the charged ions and electrons can interact directly with the solid material and possibly cause etching, it is also useful to evaluate the electron number density, which can be obtained by analyzing the Stark broadening of emission peaks. Although extensive literature exists on LIBS of

monolithic solids, this paper focuses on plasma formation associated with energetic removal of metal particles from optic surfaces to elucidate particle-substrate energy coupling, and is the first study of its kind to our knowledge.

The aim of this work is to use time-resolved emission spectroscopy to probe the early phase of the plasma formation associated with fused silica surface-bound metal particles. The plasma temperature (T_e) and electron number density (N_e) were measured throughout this threshold power-density region, and compared with the surface morphology of the substrate. We show that Fe(I)-derived temperatures scale approximately linearly with laser energy, while temperatures associated with Si(II) emission from substrate etching are significantly higher. This suggests that the plasma may be confined between the optic and the particle, leading to more effective heating than would be anticipated through monolithic plasma measurements. It is further shown that the contribution to the plasma from the optical substrate and contaminant evolves over time, yielding more substrate ions at later times. The insights gained from the analysis presented here can ultimately be used to understand better the debris mediated surface modification and to advance the understanding of laser-matter coupling relevant to debris-induced laser damage.

2. EXPERIMENTS

2.1 Sample preparation

The sample was prepared by dispersing metal particles (316L stainless steel, aluminum or tungsten) onto the exit surface (relative to laser beam propagation) of a polished and lightly HF etched UV-grade Corning 7980 fused silica window (10 mm thick by 50 mm diameter round).

2.2 Time-resolved plasma spectroscopy

Using a typical LIBS configuration,[12] the plasma emission is temporally resolved to measure the plasma temperature decay time during the plasma expansion. The experiments were carried out using a Q-switched, pulsed Nd:YAG laser system (Big Sky Laser Technologies Inc.) operating at a wavelength of 1064 nm. The single shot pulse duration of the laser system was 10 ns while the pulse energy could be adjusted using a $\lambda/2$ wave plate to fluences up to 252 J/cm^2. The pulse energy was measured by using a power meter that was placed between L1 and L2 in the experimental setup. The laser beam was guided to a focusing lens with a focal length of f=100 mm. The position of the beam waist was set onto the sample exit surface with a $1/e^2$ diameter of ~100 μm. Beam-particle alignment was achieved using a 5X objective lens coupled to a CCD camera. The laser-induced plasma emission was collected by an objective lens (10x/0.28NA Mitutoyo M Plan APO) oriented at 90 degrees relative to the beam path as indicated in Fig. 1. Light was then coupled into the end of a 19 bundle optical fiber with a core diameter of 100 μm and NA of 0.22 which is placed at the entrance slit of a Czerny–Turner spectrometer (SPEX Industries Model 270M). Spectral emission was detected by a 1024x1024 pixel intensified charge-coupled camera (PI MAX 3 ICCD). This detection system provided a spectral window of 20 nm and average spectral resolution of 0.04 nm using a 1200 gr/mm diffraction grating. Gating the ICCD with the photodiode (PD) and varying the delay time allowed for the spectra to be temporally resolved. The gate width was varied between 10 and 100 ns.

2.3 Time-resolved shadowgraph imaging

In parallel to the plasma imaging setup, a time-resolved shadowgraph imaging system was also constructed (Figure 1). This imaging system has been described in detail elsewhere.[13] Nominally spherical 316L stainless steel particles particles having a diameter on the order of 30 μm were dispersed on the exit (output) surface of 5-cm round, 1-cm thick fused silica optical windows (referred to as substrate). The substrate was positioned vertically, thus the gravitational force on the particles was parallel to the surface of the substrate. The two probe beams having their polarization orientation orthogonal with respect to each other were first combined and thereafter the combined beam was split to illuminate the particle along

the two orthogonal orientations of each microscope. Each probe pulse was delayed with respect to the peak of the pump pulse, and used as strobe illuminators to capture time resolved images by the dual axis microscope with temporal resolution determined by the probe pulse durations. The pump laser was operating at 1064 nm (1ω). The diameter of the pump beam at the particle location (exit surface of the substrate) was on the order of a few hundred μm, thus significantly larger than the size of the particles. The particles were positioned in this position of peak intensity of the beam for the execution of the experiments. The 3ω beam profile was elliptical (due to the 36 degrees angle of incidence of the laser beam) having a major axis of about 455 μm and minor axis of about 315 μm. The 3ω beam is nearly flattop with its local intensity varied within ±25% of the mean intensity.

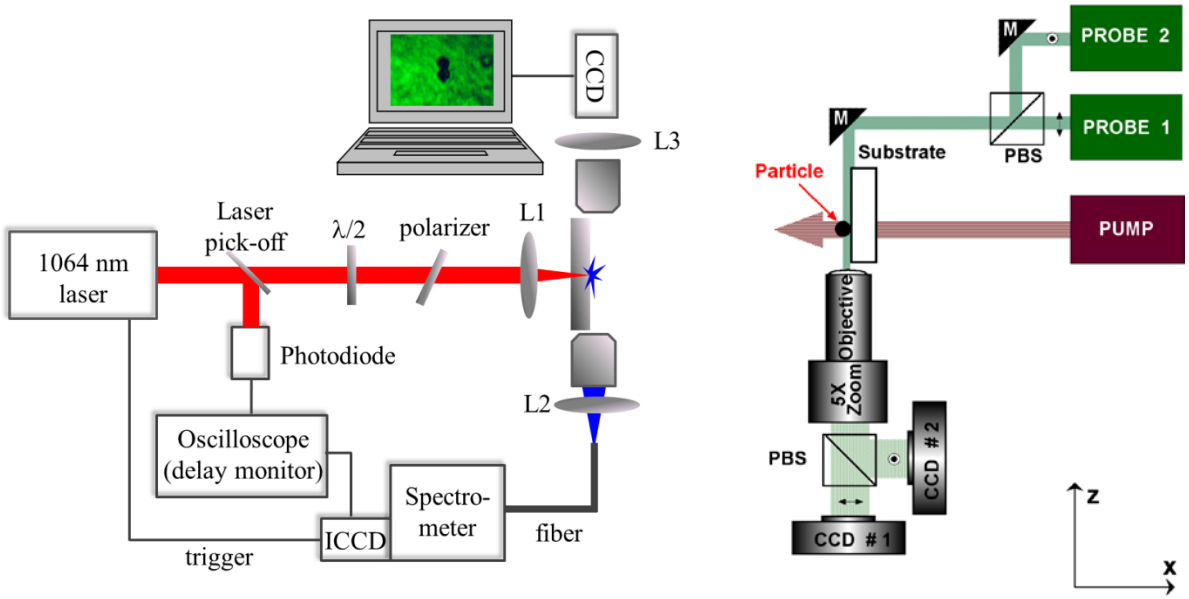

Figure 1 Time-resolved plasma spectroscopy setup (left) and time resolved shadowgraphic microscopy (right). Laser pulse energy is controlled by a wave plate and polarizer and focused (L1) at the exit surface of the SiO_2 sample where ~30 mm 316L stainless steel particles are deposited. Plasma spectrum is collected at a 90° angle using a 19-core fiber bundle and recorded with a gated ICCD camera. The ICCD is trigged by the signal from the laser. The camera delay can be varied manually and monitored against the laser pulse on the oscilloscope. A separate CCD is setup to locate and image single particles on sample surface.

2.4 Substrate surface morphology

The lateral and depth of the pits on the substrate surface resulted from laser-particle interaction were characterized using scanning laser confocal microscopy (Keyence VK-X110).

3 RESULTS

3.1 Plasma temperature and electron number density

For plasma imaging, 316L stainless steel (SS316L) particles ~30 μm in diameter were used unless stated otherwise. The typical plasma emission spectra from SS316L particle on silica substrate, SS316L plate and silica substrate only were presented in Figure 2. Two strong Fe(I) emission lines and one Si(II) emission line (substrate) were used for estimate electron temperature and electron number density.

The plasma emission spectral range selected for analysis was between 400-440 nm (See Fig. 2). This range allowed us to measure the intensity of strong Fe(I) and Si(II) emission lines and to monitor not only

the laser -particle interaction, but also the laser-substrate, and particle-substrate interactions. Furthermore, individual lines were selected based on the following criteria: 1) Measured line and background (continuum) emission should have reasonable signal-to-noise ratio, 2) Accurate spectral efficiencies from NIST must be available 3) the accuracy of the spontaneous transition probability is relatively high. Regarding signal-to-noise, we note that spectra are dominated by continuum emission in the first tens of nanoseconds after the onset of plasma, but eventually fall to levels close to the noise background.[14]

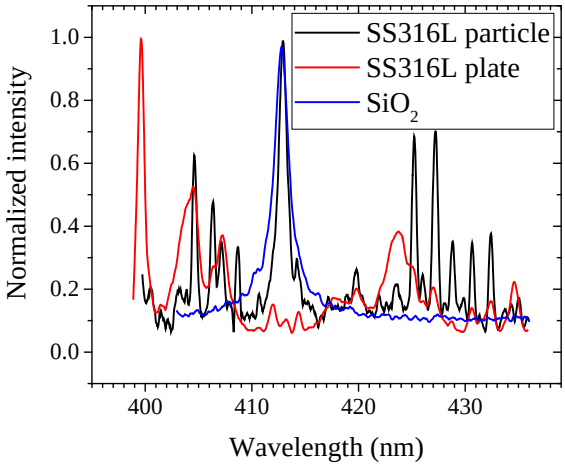

Fig. 2 Typical plasma spectra from SS316L particle on SiO_2 substrate, SS316L plate and SiO_2 substrate irradiated with single 1064 nm laser pulse.

Therefore, our measurements were limited to time delays between about 30 and 250 ns. The lines selected for plasma spectral analysis were Fe I 407.17 nm and Fe I 427.17 nm for the stainless steel particles and Si II 413.09 nm for the substrate. According to the NIST Atomic Spectra Database these lines are very intense, have highly accurate transition probabilities, and in our spectral window are free of spectral interference from other lines while their associated continuum emission could be detected at delay times greater than 100 ns.

A number of methods exist for extracting the plasma temperature and electron number density.[12,15,16] We chose the line-to-continuum (LTC) method in order to assess T_e, n_e over a relatively limited spectral range in which multiple species of interest were present. Here we assume that we our plasma is at local thermodynamic equilibrium (LTE), which will be verified later. This approach is often used in laser ablating silica interactions however, so far there is not much literature utilizing LTC for metals and alloys.[18] According to Bastiaans et al.,[19] the line to continuum ratio is

$$\frac{\varepsilon_l}{\varepsilon_c}\left(\lambda_0\right) = C_r \frac{A_{mn} g_n \lambda_c^2}{U\left(T\right)\lambda_l T_e \xi} \exp\left(\frac{E_{ion} - E_n}{kT_e}\right) \quad (1)$$

where ε_l is the line radiation intensity, ε_c is the continuum radiation intensity, C_r = 2.005 x 10^{-5}, A_{mn} is the spontaneous transition probability, g_n is the degeneracy of the upper level energy level, λ_c is the central wavelength of the emission line, E_{ion} is the ionization energy, E_n is the upper level energy level of the transition line, U(T) is the partition function of the ion, $\lambda_l \approx \lambda_c$, T_e is the plasma temperature, ξ is the free-bound continuum radiation factor and k is the Boltzmann constant. This method has the merit that an intensity calibration is not required due to the fact that $\lambda_c = \lambda_l$. A Lorentzian curve must be fitted to each spectrum when applying this method.[11] In addition to the LTC approach we also checked our temperature

estimate with the Boltzmann two-line method. By selecting two spectral lines at 407.17 nm and 427.17 nm and taking the ratio of their line intensities we can get:

$$\frac{I_{mn}^{'}}{I_{mn}} = \frac{g_{mn}^{'} A_{mn}^{'} \lambda_{mn}}{g_{mn} A_{mn} \lambda_{mn}^{'}} \exp\left(-\frac{\left| E_n^{'} - E_n \right|}{kT_e} \right) \tag{2}$$

where I_{mn}, g_n, A_{mn}, and E_n are the intensity, upper level degeneracy, spontaneous transitional probability and upper level energy of two spectral lines, respectively. It should be noted that the greater the gap between the upper level energy levels of the selected lines the, the better the accuracy of the temperature measurement.[17]

We first examined the temporal dependence of the plasma temperature associated with SS316L micro-particle on fused silica surface as plotted in Figure 3. We chose the line-to-continuum (LTC) method and the Stark broadening effect in order to assess the plasma temperature and electron number density, respectively, over a relatively limited spectral range in which multiple species of interest were present. Here we assume that our plasma is at local thermodynamic equilibrium (LTE), where $T_{exc} \approx T_e$.[18] Although the vast majority of plasma studies of laser-ablated metals are performed over micro- to milliseconds for applications such as pulsed laser machining,[19-20] we are interested in the nanosecond timescale over which the plasma and particle may interact (i.e. before the ejection process sends the particle out of the laser-generated plasma). Assuming a ~0.7 reflection loss, typical for 1 μm reflection from stainless steel spheres[21] and all the absorbed energy is converted to particle kinetic energy, an upper limit particle velocity of ~2 km/s is obtained for a 10 GW/cm^2 pulse, resulting in a lower limit time frame of ~15 ns. 75 individual (single shot) measurements were taken over a 50 – 215 ns range with 10 ns gating revealing temperatures near 24,000 K (2.1 eV) at short times which decays to ~15,000 K (1.3 eV). Previous studies on laser ablation of FeNi alloys[22] yielded a τ^{-p} power dependence of p=0.22, where as in the present case p=0.28±0.025. In most cases the plasma temperature for stainless steel decreases rapidly (sometimes exponentially) at early stages of plasma expansion and maintains a relatively constant temperature thereafter.[14]

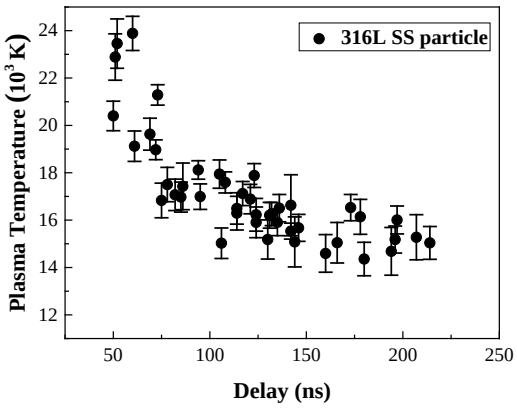

Figure 3. Plasma temperature as a function of gate delay for a SS316L steel particle on SiO_2 substrate irradiated with single 1064 nm, ~10 GW/cm^2 laser pulse.

The temperature drop for an adiabatic gas cloud expansion scales as $T \sim 1/t^{3(\gamma-1)}$ where γ is the gas adiabatic constant.[23] The adiabatic constant can be expressed as γ=(N+2)/N where N is the atom's degrees of freedoms. Atomic ionization produces the multiple additional degrees of freedoms and for an ionized gas the adiabatic constant is near unity. Usually, for description of an ionized gas the γ values in the range

1.1-1.2 are used.[23] The value γ =1.1 is consistent with our data. The slower rate of cooling is consistent with the behavior of confined plasma and can be explained by the energy re-deposition from the plasma recombination. The fast decay at the early dense stage can be related to the radiative cooling because the plasma is dense and hot resulting in very efficient radiative cooling. However at later times, the temperature and electron density drops, the photon mean free path becomes longer than plasma size and the role of the radiative cooling becomes less dominant.

To investigate the energy-dependent removal of silica caused by the laser ablation of surface bound metal particles, we used the LTC method to evaluate simultaneously the temperature associated with Si(II) and Fe(I) species generated within the ~600 μm collection area of our spectral imaging system. Figure 4 shows the temperature derived from each species as a function of laser intensity plotted on a log-log scale for a gate delay of 222 +/- 8 ns. The Fe ions appear to increase from ~15,000 K at about 5 GW/cm^2 to ~29,000 K near 35 GW/cm^2, increasing as ~580 K-GW^{-1}cm^2. On the other hand, Si ion temperatures – only measurably above 10 GW/cm^2 due to low 413.1 nm emission line strength - appear much hotter, ranging from ~36,000 to ~40,000 K over 11 to 35 GW/cm^2 laser intensities with a slope approximately half that for Fe (~230 K-GW^{-1}cm^2). Because the removal of Si atoms occurs over a region smaller than the diameter of the particle, the results suggest that the plasma within the gap between the ejected particle and substrate may be confined and thus driven to higher temperatures than under weakly confined conditions.

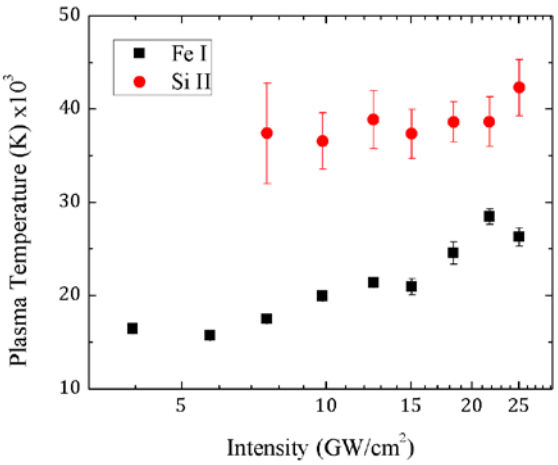

Figure 4. Comparison of temperatures as a function of laser intensity extracted from plasma emission lines related to the substrate (fused silica, Si(II)) and the ejected particle (SS316L, Fe(I)).

The simultaneous observation of Si and Fe emission spectra allows us to estimate the relative concentration of species created during the ablation process. Figure 5 shows the peak intensity ratio Fe(I)/Si(II) as a function of laser pulse intensity, after normalizing by the Boltzmann factor, $e^{-E/kT}$ to correct (to first order) for differences in excited state populations of the two species. The decrease in normalized Fe signal relative to that of Si is observed with increasing irradiance as Si atoms are produced as more energy is coupled into the substrate, removing silica material.

Because the etching potential of a plasma is influenced by both temperature (ion energy) and charged species density (dosage),[24] we evaluated the electron number density, N_e, and compare it to the material removal rate as a function of laser intensity. N_e was estimated by measuring the Stark broadening of the 427.17 nm emission lines for Fe(I) and 413.08 nm for Si(II). The electron number density, N_e, is given by[25]

$$N_e = \frac{\Delta\lambda_{FWHM}}{2W} \times 10^{16} \quad (3)$$

where $\Delta\lambda_{FWHM}$ is the Lorentzian Full width half maximum, otherwise known as the Stark width, and W is the electron impact parameter which is a function of the plasma temperature.

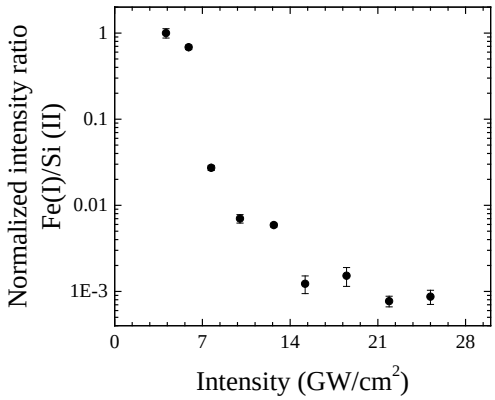

Figure 5. Natural log of the Boltzmann-normalized peak intensity ratio of [Fe (I) 427.17nm]:[Si II 413.09 nm] as a function of laser intensity at a gate delay of 220 ns.

Table I displays N_e for 5.9, 7.7 and 10 GW/cm^2 laser intensity, along with plasma temperature in K, and substrate ablation depth in nm. As discussed earlier, when laser light irradiates the metal particles after passing through the silica interface, Fe atoms are ejected through evaporation over virtually all of the πa^2 cross section. For this reason, we see large fluctuations for the particle electron number density as the laser-particle irradiance may not be as uniform compared to the laser-substrate irradiance. Furthermore, recent studies on particle-plasma interactions speculate that during the first few nanoseconds of plasma expansion one side of the particle is subjected to a greater radiant flux and may consequently under a faster rate of vaporization.[26] As a result, 1) significant momentum may be transferred to the remaining solid particle, which like thermophoresis may displace the particle to less energetic plasma regions 2) the particle may not have time to expand and heating occurs at nearly constant volume 3) constant volume heating induces a pressure buildup that may fracture and break particles into smaller pieces which are readily vaporized with in the plasma volume. On the other hand, the ablation depths increase nonlinearly as more energy is partitioned into removing SiO_2 and creating a Si-rich plasma, with a rapid increase at low energy due to efficient confinement.

Table 1. Electron number density and plasma temperature for Fe and Si atomic species in the plasma as a function of laser irradiance along with the final pit depth and the ejected particle kinetic energy.

Laser irradiance (GW/cm^2)	Electron number Density (x10^{17} cm^{-3})		Plasma Temperature (x10^3 K)		Ablation pit depth (nm)	Particle velocity (m/s)
	Fe	Si	Fe	Si		
5.9	3.55±0.08	0.31±0.01	15.7±0.2	-	513±173	35±17
7.7	4.21±0.17	0.54±0.003	17.5±0.2	37.4±0.5	1068±601	48±16
10	4.39±0.30	0.53±0.003	19.9±0.4	36.5±0.3	1270±750	68±24

3.2 Pit formation on silica substrate

It is well-known that at low enough laser energy (<0.1 J/cm^2 or <10 MW/cm^2), attached particles may be "dry" laser cleaned from surfaces with negligible surface damage.[21] However, it is natural that at fluences sufficient to generate plasma from attached metal particles, some energy may couple into the substrate surface causing damage. Figure 6 displays the morphology (measured using laser-scanning confocal microscopy) of two pits created from a ~2.4 and 7.7 GW/cm^2 pulses. We note that the profiles are smooth, in contrast to more typical, exit surface laser-induced damage which tends to display significant fracture.[27,28] While smooth pitting can be created through thermally-induced glass relaxation mechanisms

leading to densification,[29] our experiments confirmed that Si atomic species are also present in the laser-generated plasma, indicating vaporization and ionization of material by the hot plasma as the root cause of pitting at high fluences (>0.1 J/cm^2). It is not surprising that both the pit depth and width increase as increasing laser intensity. A big variation in depth and width was also observed possibly reflecting the individual particle thus the plasma confinement condition.

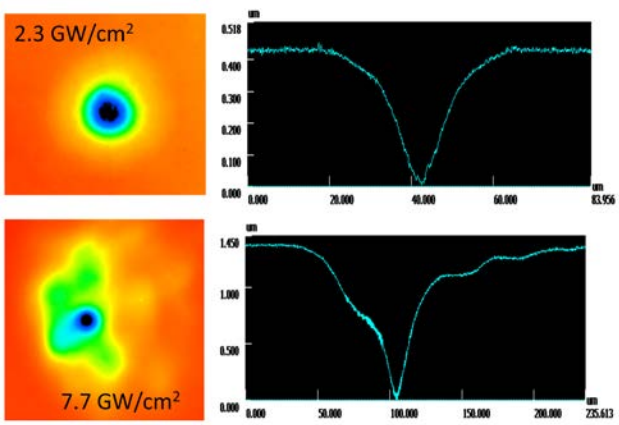

Figure 6. Confocal images and depth profiles of surface pits formed by laser ejection of SS316L particles at two laser intensities.

3.3 Particle ejection and response

Figure 8 shows the speed of ejection of SS316L particles as a function of the laser peak fluence. The onset of ejection of particles is observed to be at about 2.4 J/cm^2 where only a small fraction of the particles (<10%) was observed to eject from the surface. On the other hand, nearly all particles (>95%) were ejected from the substrate at about 13.5 J/cm^2.

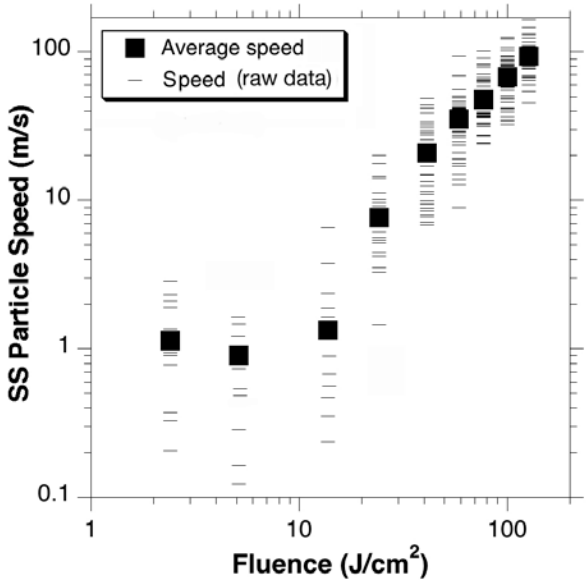

Figure 7. Raw data (bar) and average speed (solid square) of ejection from the substrate of SS316L particles as a function of the laser fluence.

Interestingly, the average speed of ejection of the particles in this range is nearly constant, at about 1 m/s. This seems to indicate that the process involved in all cases is similar and may be related to a threshold energy required to be attained by the particles in order to overcome the van der Waals forces responsible for the adhesion of the particles on the substrate. Above this fluence, a rapid increase of the speed of the ejected particles as a function of laser fluence is observed. The particles reach a speed on the order of 100 m/s for at fluence on the order of 150 J/cm^2 as shown in Figure 7.

Although the speed of the particles can be high, it is more than one order of magnitude lower than the speed of the shockwave generated by the process of laser energy deposition on the particle surface. This behavior is exemplified by the time resolved image shown in Figure 8a captured at 500 ns delay where both, the transient location of the shockwave and the metal particle are observable. I addition, a liquid material "spray" is observed to transverse around the particle. We postulate that this is related to the melted material on the surface of the particle that was atomized and captured by the aerodynamic flow of the hot gas flow around the particle. This behavior was also observed in other types of metal particles, such as in the example of aluminum and tungsten particles shown in Figures 8b and 8c. These two cases demonstrate that a much larger amount of liquid "spray" is generated in the aluminum than in tungsten, which is believed to be related to the amount of liquid material (due to the corresponding thermodynamic properties) generated in each type of metal particle.

A detail investigation of the processes involved in the interaction between the laser beam and the particle and substrate will be discussed elsewhere. However, in this work we want to highlight the importance of the stresses exerted on the particles during this process. These stresses can exceed the mechanical strength of the particle, which can lead to its partial or complete fragmentation. This behavior is exemplified by the images shown in Figures 8d and 8e. Specifically, Figure 8d demonstrates the fragmentation of aluminum particles at a fluence of 60 J/cm^2. At higher fluence, the number of fragments increases and at about 100 J/cm^2 a complete fragmentation of particles was often observed (see example in Figure 9e).

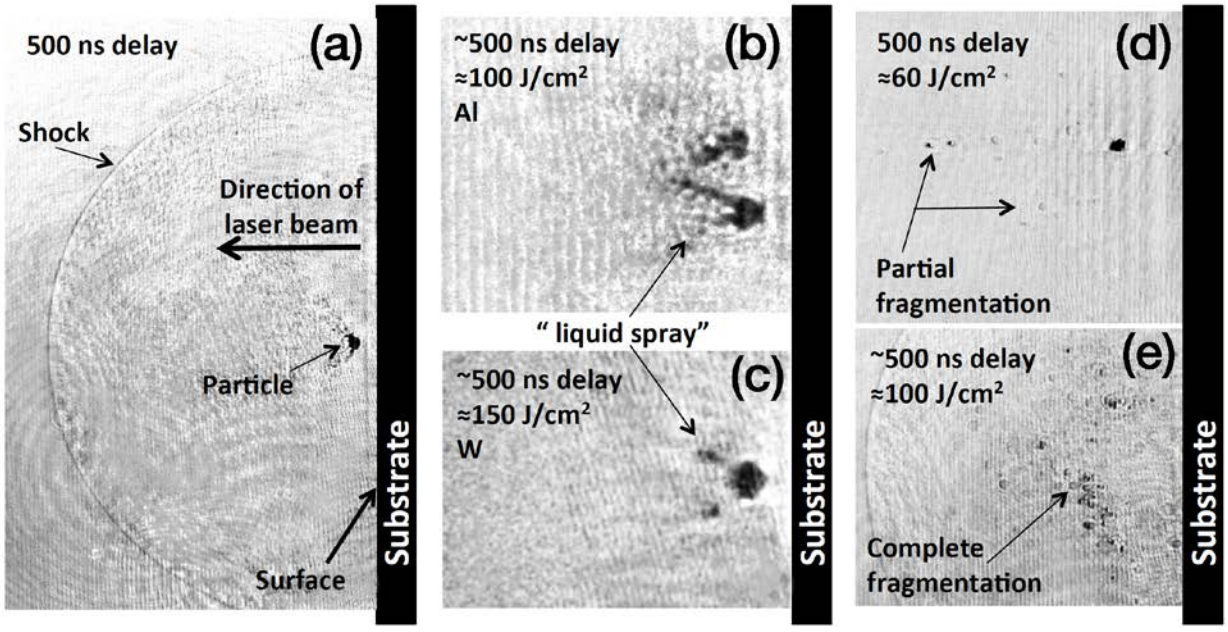

Figure 8. Time resolved images captured at 500 ns delay (prom peak of pump pulse) of metal particle response to exposure to ns laser pulses. (a) SS316L particles showing the position of the particle and shockwave. (b) Aluminum and (c) Tungsten particles showing the formation of a "liquid spray" that travels around the particles. Aluminum particles exhibiting (d) partial and (e) complete fragmentation, depending on the laser fluence.

4 CONCLUSION

In conclusion, the ejection of silica surface bound steel particles by way of energetic laser pulses is shown to be accompanied by plasma containing both Fe and Si atomic species. A higher plasma temperature was extracted from the Si species relative to that of Fe, consistent with the generation of a confined Si-rich plasma at the particle-substrate interface. Shadowgraph-based plasma imaging and ejection velocity measurements further support the physical picture of confinement over the laser intensities studied, and imply an enhancement of material removal rate and surface damage due to particle ablation. Radiation reflection and plasma confinement effects in the region between the escaping particle and the substrate will enhance the laser-plasma coupling and drive the plasma to higher temperatures and electron number densities that lead to vaporization and etching of substrate material. These results are relevant to laser-induced surface pitting associated with metal contaminants on high power laser optics,[30] and provide insight into the origins of pitting dependence on pulsed laser energy.

ACKNOWLEGEMENTS

This work performed under the auspices of the U.S. Department of Energy by Lawrence Livermore National Laboratory under Contract DE-AC52-07NA27344. This work was funded by the Laboratory Directed Research and Development Program at LLNL under project tracking code 14-ER-098. [LLNL-CONF-679001]

REFERENCES

1. G. Vereecke, E. Rohr and M. M. Heyns, J. Appl. Phys. **85**, 3837-3843 (1999).
2. A. Kumar, R. B. Bhatt, M. Afzal, J. P. Panakkal, D. J. Biswas, J. P. Nilaya and A. K. Das, Nucl. Technol. **182**, 242-247 (2013).
3. A. Vatry, M. N. Habib, P. Delaporte, M. Sentis, D. Grojo, C. Grisolia and S. Rosanvallon, Appl. Surf. Sci. **255**, 5569-5573 (2009).
4. S. Palmier, S. Garcia and J. L. Rullier, Opt. Eng. **47**, 0842031-0842037 (2008).
5. J. Honig, M. A. Norton, W. G. Hollingsworth, E. E. Donohue and M. A. Johnson, Proc. SPIE **5647**, 129-135 (2005).
6. F. Y. Genin, M. D. Feit, M. R. Kozlowski, A. M. Rubenchik, A. Salleo and J. Yoshiyama, Appl. Opt. **39**, 3654-3663 (2000).
7. M. J. Matthews, N. Shen, J. Honig, J. D. Bude and A. M. Rubenchik, J. Opt. Soc. Am. B **30**, 3233-3242 (2013).
8. D. Grojo, P. Delaporte, M. Sentis, O. H. Pakarinen and A. S. Foster, Appl. Phys. Lett. **92**, 033108-033111 (2008).
9. N. Shen, J. D. Bude and C. W. Carr, Opt. Express **22**, 3393-3404 (2014).
10. S. Palmier, J. L. Rullier, J. Capoulade and J. Y. Natoli, Appl. Opt. **47**, 1164-1170 (2008).
11. S. Zhang, X. Wang, M. He, Y. Jiang, V, W. Hang and B. Huang, Spectrochim Acta B **97**, 13-33 (2014)
12. .H. C. Liu, X. L. Mao, J. H. Yoo and R. E. Russo, Spectrochim Acta B **54**, 1607-1624 (1999).
13. R. N. Raman, R. A. Negres and S. G. Demos, Opt. Eng. **50**, 013602 (2011).
14. H. Y. Moon, B. W. Smith and N. Omenetto, Chem Phys **398**, 221-227 (2012).
15. C. Aragon and J. A. Aguilera, Spectrochim Acta B **65** (5), 395-400 (2010).
16. X. Z. Zeng, X. L. Mao, S. S. Mao, J. H. Yoo, R. Greif and R. E. Russo, Journal of Applied Physics **95** (3), 816-822 (2004).
17. Q. L. Ma, V. Motto-Ros, X. S. Bai and J. Yu, Appl. Phys. Lett. **103** (20) (2013)
18. G. J. Bastiaans and R. A. Mangold, Spectrochim. Acta B **40**, 885-892 (1985).
19. R. E. Russo, A. A. Bol'shakov, J. H. Yoo and J. J. Gonzalez, Proc. SPIE **8243,** 82430A–82430A–7 (2012).
20. G. Sarri, K. L. Lancaster, R. Trines, E. L. Clark, S. Hassan, J. Jiang, N. Kageiwa, N. Lopes, R. Ramis, A. Rehman, X. Ribeyre, C. Russo, R. H. H. Scott, T. Tanimoto, M. Temporal, M. Borghesi, J. R. Davies, Z. Najmudin, K. A. Tanaka, M. Tatarakis and P. A. Norreys, Phys. Plasmas **17**, 113303 (2010).

21. G. G. Gladush and I. Smurov, *Physics of Laser Materials Processing* (Springer-Verlag, 2011).
22. J. A. Aguilera and C. Aragon, Spectrochim Acta B **63**, 784-792 (2008).
23. Ya.B. Zeldovich and Yu.P. Raizer, *Physics of shock waves and high-temperature hydrodynamic phenomena* (Dover, 2002).
24. Y. F. Lu, W. D. Song, K. D. Ye, M. H. Hong, D. M. Liu, D. S. H. Chan and T. S. Low, Appl. Surf. Sci. **120**, 317-322 (1997).
25. H. R. Griem, *Spectral Line Broadening by Plasmas* (Academic Press, 1974).
26. J.E. Carranza and D.W. Hahn, Anal. Chem. **74**, 5450-5454 (2002).
27. M. J. Matthews, C. W. Carr, H. A. Bechtel and R. N. Raman, Appl. Phys. Lett. **99**, 151109 (2011).
28. J. Wong, J.L. Ferriera, E.F. Lindsey, D.L. Haupt, I.D. Hutcheon and J.H. Kinney, J. Non-cryst Sol. 352, 255-272 (2006).
29. Y. F. Lu, W. D. Song, K. D. Ye, Y. P. Lee, D. S. H. Chan and T. S. Low, Jpn. J. Appl. Phys. 2 **36**, L1304-L1306 (1997).
30. E. Feigenbaum, S. Elhadj and M. J. Matthews, Opt. Express **23**, 10589-10597 (2015).